STAR Note # 250

June 1996

Simulation of the End–cap Calorimeter for STAR Detector.

K.S.Medved

Visitor to Brookhaven National Laboratory from JINR, Dubna, Russia

W.B.Christie

Brookhaven National Laboratory

Abstract

The installation of the End–cap Electromagnetic Calorimeter (EEMC) would significantly increase the physics capabilities of the STAR detector to study spin–dependent processes. In this paper, the first results of software simulations for EEMC are presented. A geometrical description of the EEMC, and some simple hints of how to extract the EEMC information in GEANT, are explained.

The basic characteristics of the EEMC, such as the resolution and energy losses due to cracks and inefficient regions, were studied. The possible influence of extra material (TPC Wheel) on the EEMC response was simulated, and some suggestions for the EEMC design are offered.

1 EEMC : motivation, capabilities and design.

The existing data on nucleon spin structure functions obtained in several experiments on deep inelastic scattering led to the conclusion that constituent quarks are not the single carriers of the nucleon spin [1]. This situation is often referred to as the "spin crisis". The remaining spin of the nucleon is some combination of the spin of the gluons and sea quarks, and the orbital angular momenta of the valence quarks. The existing experimental data is insufficient to make a choice in favor of a single theoretical explanation of the phenomena.

The characteristics of the future RHIC collider (energy, luminosity, high degree of proton beams polarization) give unique possibility to study the spin dependent structure functions, in particular the contribution of the *gluon and sea quark* components to the total spin of the proton [2]. These spin studies are part of the scientific program of the STAR experiment.

At present, only theoretical estimates of the gluon spin dependent structure function exist. It is also known that several reactions are probably sensitive to the behavior of gluon spin structure function $\Delta G(x)/G(x)$. The most straightforward method [1] of studying the gluon spin structure function is, probably, its extraction from the measured small spin asymmetries in reaction $\vec{p} + \vec{p} \longrightarrow \gamma^{\star} + jet + X$. The accuracy expected from the STAR data is estimated at the level of $\delta(\Delta(G)/G)) = 0.02$.

From the experimental point of view, these studies require the installation inside the STAR magnet of an electromagnetic calorimeter with large kinematical acceptance, good energy resolution, and minimal and correctable losses. The plan of the Collaboration for building the Barrel Electromagnetic Calorimeter (**BEMC**) is already well determined. The acceptance of the BEMC covers two units on pseudorapidity $-1 < \eta < +1$, and 2π in azimuth. Assuming the average jet size $\sim \sqrt{\eta^2 + \phi^2} = 0.7$, the effective acceptance of BEMC for jets is only $-0.3 < \eta < +0.3$. The obvious and comparatively inexpensive way of extending the jet acceptance is the construction of an End–cap Electromagnetic Calorimeter (**EEMC**) with the coverage of $+1 < \eta < +2$. This will extend the acceptance

[1] Other methods, sensitive to $\Delta G(x)$ include : registration of J/Ψ, D-meson studies, observation of 3– and 4– jet events [2, 3]. The reaction (direct γ + side–away jet) is the most simple approach to the problem.

for jets up to $-0.3 < \eta < +1.3$. A schematic view of the STAR detector with both BEMC and EEMC installed is shown on Fig.1.

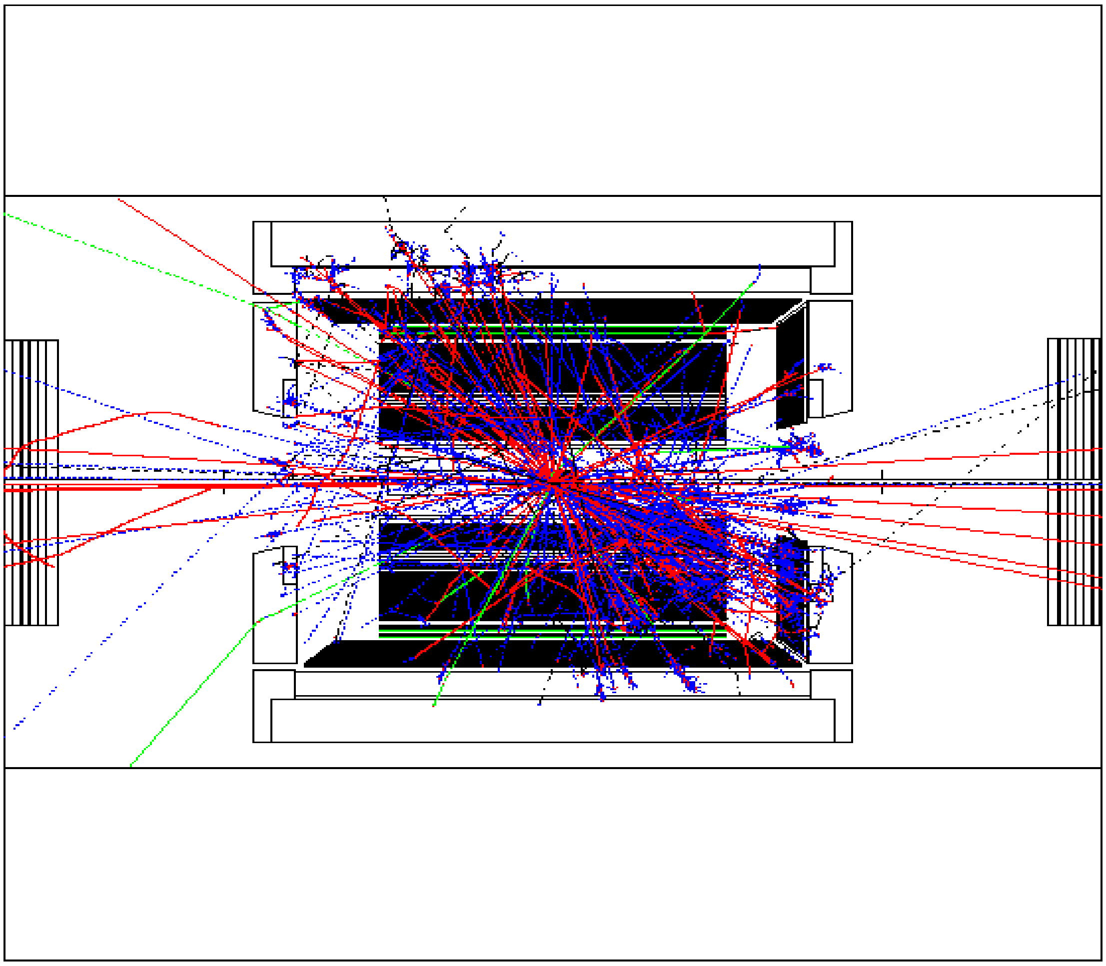

Figure 1:

Schematic view of STAR detector. Positions of BEMC and EEMC are shown in black color. This is an example of pp–interaction at $\sqrt{s}$ *= 200 GeV. The particles of a high-* p_T *jet (lower right corner) hit both the BEMC and EEMC.*

There are two groups working on possible design for an EEMC. One of the possible options, based on a mechanical design of Argonne National Laboratory, was recently presented by Penn State University [4]. This paper contains a good review of physical processes underlying the STAR spin program, and the detailed explanation of the PSU Project Plan.

Another option is based on the design suggested by the Particle Physics Laboratory (JINR, Dubna). This project is also considered by the Collaboration, and detailed drawings of the PPL EEMC are available on the BNL/RHIC computer cluster [2].

The mechanical details of the two designs are different. Nevertheless, most of the basic properties of the EEMC are determined by the geometrical size and position of the EEMC envelope (fixed by the Integration Group requirements [5]). Also, in both proposals it is assumed that EEMC is a lead–scintillator calorimeter, similar to the BEMC design.

This is the reason why at the *simulation* level (i.e. at the level of geometrical description in GEANT, where some mechanical details are necessarily omitted), the difference between various designs is small. In this paper, most of the simulation results were obtained using the PPL EEMC design.

The End-cap ElectroMagnetic Calorimeter is a lead–scintillator calorimeter composed of 720 towers. Each single tower covers $\Delta\phi \simeq 0.1$ (6^o) and $\Delta\eta = 1/12 \simeq 0.08$. The tower has a trapezoidal form, with the size of a scintillator tile $16 \times 14 cm^2$ at the average EEMC radius [3] of 160 cm.

[2]There are three big sets of drawings :
in directory ~**shvetsov/eemcdraw** there are drawings explaining the design of EEMC itself. Please note, that several options for tower geometry are presented. Drawings are available as *.eps and *.dwg files (CAD format).
Directory ~**shvetsov/stress** contains the set of pictures showing the distribution of stresses in the construction elements of EEMC, obtained as the results of calculations using the method of finite elements.
Directory ~**shvetsov/holepatt** contains the very detailed pictures of EEMC support structure and the details of module mounting to STAR magnet pole tip.

[3]The question of how the interval $1 < \eta < 2$ will be divided for EEMC, is still under discussion. There are two opportunities :
– divisions with equal $\Delta\eta$, but different heights;
– divisions with equal heights ($(R^{EEMC}_{max} - R^{EEMC}_{min})/12$), but slightly different $\Delta\eta$.
In principle, ideal projective geometry (where axis of each EEMC tower will point to the interaction vertex) would require manufacturing of large variety of scintillator tiles of different sizes, ant it will rise the production cost dramatically. In this sense, the EMC design is a compromise between the cost, simplicity, and reasonable physical characteristics.

The construction of the EEMC is illustrated in Figure 2, where the cross section of *one* tower is shown. The Integration Group requirement limits the total thickness of the EEMC by 38.7 cm. Out of this number, 6 cm should be used for strong back support plates. Each EEMC tower consists of 26 scintillator layers (each 4 mm thick) and 23 lead layers (each 5 mm thick). After the 6th scintillator layer, the ShowerMax Detector (SMD) is located. The total thickness of all lead and scintillator layers is 21 radiation lengthes. Taking into account the material of internal support structures, the EEMC thickness is
$\sim$ **22 radiation length**.

Mechanically, the EEMC is divided into twelve 30^o *modules*. Each module consists of 60 towers and is mounted independently onto the magnet poletip.

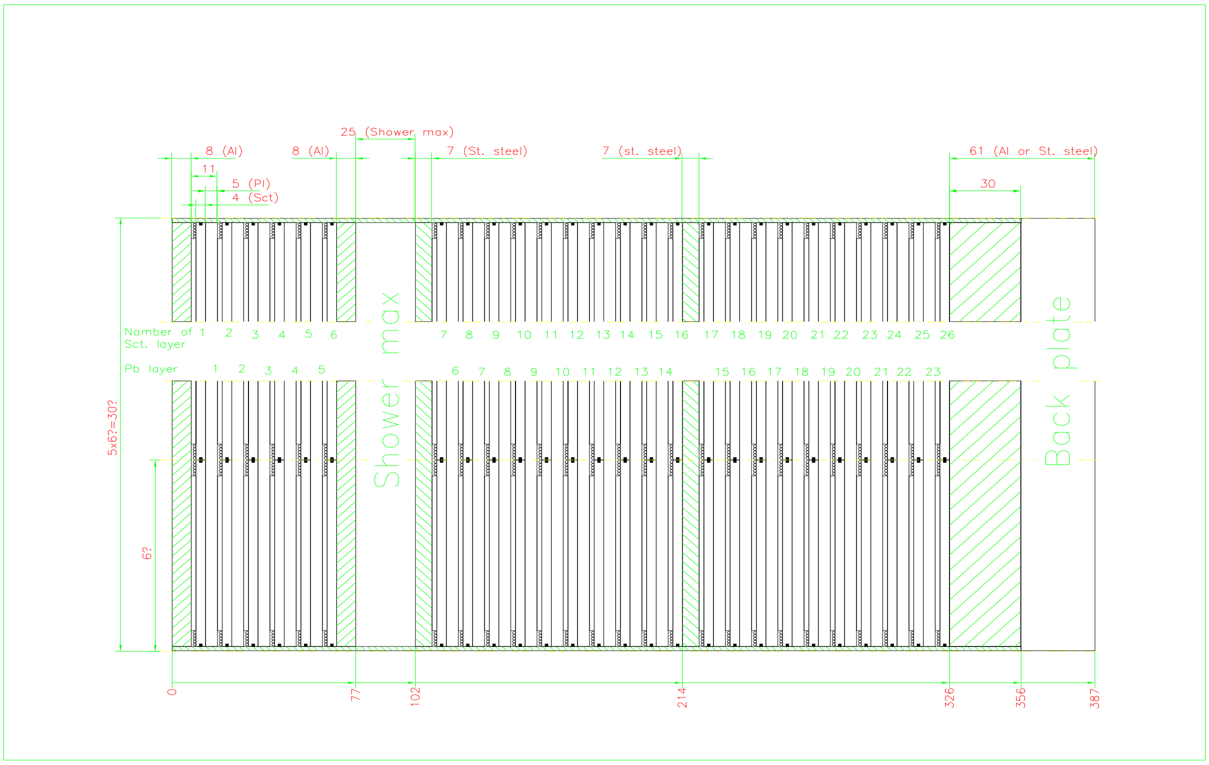

Figure 2:

The design of one EEMC tower is shown. The tower consists of 23 lead layers and 26 scintillator layers. The total thickness is 22 X_o.

2 EEMC : geometry files.

There have been three geometrical descriptions of the EEMC implemented in GEANT.

The "old" GEANT.

The namelist file $STAR_REF/sim/mcg/geo/emc/emc_barrel_endcap.geo was the first iteration in GEANT of the EEMC geometry. In this version, EEMC is described in a simplified form : each scintillator or lead layer is described as a 2π ring, without division to modules and towers. For many studies, when one does not take care about energy losses in cracks, this geometrical description is convenient. Moreover, when nothing is known yet about the exact size and positions of individual towers, and this question is to be studied, this method is preferable. In preliminary studies, this file could be used to simulate almost any design. The sorting of hits into towers could be done later at the software level. Please note: this geometry file contains both the descriptions of the BEMC and the EEMC.

The next version of the geometry file, corresponding to the JINR design, can be found in ~medved/public/eemc/geom/emc_endcap_test01_vx.geo. In this file, the EEMC is divided into modules, and external and inner support structures are described as well. Most of the calculations presented in this paper were performed using this geometry file.

The "new" GEANT.

The geometrical description of EEMC in aGSTAR is defined in a different way. The geometrical volumes of the EEMC are determined at run–time with the help of a special **module** [6]. Before the run, the **module** is translated by a preprocessor into a standard Fortran subroutine and linked with the GSTAR libraries. The module for EEMC, written by R.Mekhdiev (JINR), can be found in $STAR_REF/sim/gst/geo/g/ecalgeo.g. This module contains a description of the EEMC down to the level of the single tiles. In this version, SMD is described as being filled with air, though the ShMax hits are available. This gives the correct distribution of hit coordinates, but the energy response of SMD pads should be treated with caution. Also, it is assumed that three groups of the longutudinal segmentation of the towers could be readout independently. This *module* can be used as a starting point for any changes of the EEMC geometry [4].

[4]There is an example .kumac-file for aGSTAR drawing the pictures of EEMC geometrical structures : ~nevski/public/star/doc/ecadoc.kumac — it draws a picture ecafig.ps (also available there).

An interesting possibility on extraction of the EEMC hits information without using the *g2t package* , during the aGSTAR run-time, was demonstrated to the authors by P.Nevski.

A working example can be found in /star/emc/medved/Nevski_example (or in /u2c/medved/public/Nevski_example).

The file README explains tips on running aGSTAR in this mode.

Several pp–events are in the input file testevt.txt.

To proceed the example, do the following :

```
cd /star/emc/medved/Nevski_example
sh kill_em
gstar

>exec geom datecal
>exec stareemc

[ ...you will see aGSTAR working and drawing pictures ... ]
>quit
```

After processing 3 events, you will get two simple files, *eehits.dat* and *smhits.dat*, containing the information about all EEMC hits. The file test.fzd contains the usual Zebra-banks.

Please note : in the current geometry version there are 2 End-caps : at +z and -z ! We are usually using the one at +z.

This example gives the basic idea of how the information from aGSTAR could be obtained during run-time. In the example, only TPC and EEMC detectors were present. To run aGSTAR with full a set of detectors, use *star.kumac*. It processes 3 pions through the complete STAR geometry.

3 EEMC : resolution and response.

The energy resolution is one of the most important characteristic of the EMC. It depends on the calorimeter material and its design. Figure 3. shows electromagnetic showers initiated by photons of various energies, as seen in GEANT. The position of the maximum of the EM shower and median depth of a shower energy deposition can be calculated using the standard formulaes [8, 9]. Median depth of a shower is the depth (in units of radiation length) by which half of the incident energy is deposited :

$t_{med} = [ln(E_\gamma/\epsilon) + 1.2) \qquad = 7.7 \qquad$ for 5 GeV γ's;

$t_{med} = [ln(E_e/\epsilon) + 0.4) \qquad = 6.9 \qquad$ for 5 GeV electrons.

The maximum of the shower (the depth at which dE/dx in a shower reaches its maximum) is related to the median depth as :

$t_{max} = t_{med} - 1.5 \qquad = 5.2\ X_0, \qquad$ for 5 GeV γ's.

Here, ϵ is called the *critical energy*, equal to 7.2 MeV for lead [8].

As an example, several longitudinal shower profiles in EEMC for γ's with energies 3 and 10 GeV are shown on Figure 4.

The calorimeter length, needed to contain 98% of the incident energy, is

L(98%) $\simeq 3t_{med} \qquad \simeq 21\ X_0 \qquad$ for 5 GeV electrons.

But, taking into account the fact that, in average, an incident particle hits EEMC at angle $\theta = 25^o$, and for scintillator the value of ϵ is higher [5], the EEMC can effectively contain a 20 GeV shower without significant losses. At higher energies, the longitudinal leaks will seriously spoil the EEMC resolution, and corrections must be applied.

Assuming that the energy resolution of the EEMC follows the law $\delta E/E = k/\sqrt{E}$, one could extract the EEMC resolution from GEANT data. To do this, a special set of events was prepared. It consisted of 2,000 $\gamma's$ with energies from 0.1 to 15 GeV. The directions of the γ's were not chosen randomly. They were required to hit the EEMC at the average radius of 160 cm, and the entry points were at the centers of the tiles, far from support walls and cracks (to avoid the lateral leakage).

[5] At $\theta = 25^o$, the effective length of EEMC is about 24 X_0. In EEMC, the angles of incidence are in the interval $[15^o < \theta < 38^o]$.
Critical energy ϵ is about 70–80 MeV for a scintillator.

The results are presented in Figure 5. The EEMC resolution was calculated [6] as $(16.5 \pm 2)\%$. This is close to the value (13%) achieved with the prototype Barrel EMC module in a test beam.

To study the angular dependence of the calorimeter resolution, a special EEMC geometry file for GEANT was prepared. The inner diameter was artificially reduces, so that incidence angles of $[2^o < \theta < 38^o]$ were allowed. As expected (due to the sampling factor) the EEMC resolution $k(\theta)$ follows the simple law $k(\theta) \sim 1./cos(\theta)$, varying from 16% at 5^o to 20% at 35^o of incidence.

In a calorimeter, some small part of energy is being scattered in a backward direction. The existing data give the estimate of the *albedo* at the order of 1% at 10 GeV. This is a small effect, and at the current level of simulation it was ignored.

Calorimeter response. In an lead-scintillator calorimeter only that part of the energy deposited in the active layers can be seen. The following table illustrates how the ratio between the "visible" and total deposited energy can be estimated (for *mip*)

```
Thickness of EEMC materials :

23*0.5 cm = 11.5 cm   Lead
26*0.4 cm = 10.4 cm   Scintillator
             7.4 cm   Air
             1.6 cm   Aluminium
             1.4 cm   Steel

Energy, deposited by a minimum ionizing particle ( mip ) :

          134.6 MeV   in Lead
           17.9 MeV   in Scintillator
            8.3 MeV   in Air
            6.1 MeV   in Aluminium
           15.0 MeV   in Steel
         ------------
          181.9 MeV   is the total deposited energy in the EEMC by a mip.

Ratio (E_scint.)/(E_total) = 0.098
```

[6] This number is the result of a least–squares fit. Though a "Bancroft Rule" [10] said :
"In order to calculate the slope of the best straight line through a set of points, simply join the first and the last point".

Presented on Figure 6a, is the sampled energy, deposited in active layers versus the energy of the incident photons. The GEANT simulation result is that $\sim$7.3% of the incident photon energy is collected.

For comparison, Figure 7b shows the same dependence, obtained using GEANT for π^+–meson and muons. The much bigger error bars for π^+ mesons [7] illustrate the fact that the fluctuations of deposited energy for hadrons are much larger than those observed for electrons or photons [8]. Muons, having a small probability to interact or start a shower inside the EEMC, leave only a minimal amount of energy (about 20 MeV in active layers, as shown in the example).

4 EEMC : walls and cracks.

The real calorimeter is not an ideal structure, consisting only of alternating lead and scintillator layers. The necessary elements of the EEMC design (supporting walls, cracks between elements, etc) create the dead regions inside the calorimeter. The conditions for collecting photoelectrons are different depending on the hit position inside the scintillator tile. The optical fiber routing also creates at the edges of a tile some regions having different light collection characteristics.

These effect distort the uniformity of the calorimeter. A study was performed to estimate to what degree these nonuniform regions influence the characteristics of the calorimeter, how large the regions are, and where they are.

For the current design of the calorimeter, all the gaps, cracks, and other irregularities mostly distort the lateral structure of EM showers. The lateral profile of an EM shower $dE(R,z)$ is a rather complicated function, and depends on the depth z along the shower axis. To get a simple estimate, let us consider the average lateral profile of a EEMC shower, integrated over z. In Fig.7, two lateral profiles, from γ's with energies of 3 and 10 GeV, are presented. The distributions can be well approximated by the sum of two exponents $dE/dR = A_1 \times exp(-R/r_1) + A_2 \times exp(-R/r_2)$. The fit gives the results $r_1 \simeq 1.2cm$

[7] as compared to those in Fig.6a.

[8] The fluctuations in hadronic showers will be discussed in more details in the forthcoming STAR Note on EEMC FastSimulator.

and $r_2 \simeq 4.5cm$, which correspond to the narrow "core" and tail of the shower. For these distributions, 95% of the shower energy is concentrated inside a radius of 5 cm.

Usually, the characteristic radius of an EM shower is considered equal to $R_m = X_0 E_s/\epsilon$, where $E_s = 21$ MeV (this follows from the multiple scattering theory), and ϵ is the critical energy. For lead, $R_m \simeq 1.6cm$. It was shown [8] that 95% of the shower energy is deposited inside the cylinder along the shower axis with the radius R(95%) $= 3 \times R_m = 4.8$ cm. This corresponds quite well to the EEMC GEANT simulation. This also gives the scale of the distance at which a dead region could start to influence the energy measurement.

In the bottom of Fig.8 an EM shower near the iron wall between modules is shown. The plots at the top of Fig.8 show the energy deposited in a EEMC tower as a function of the distance between the axis of the shower and the wall. At distances smaller than 2 cm the influence of the wall becomes significant, and the total deposited energy inside the tower decreases dramatically.

In Fig.9 an EM shower is shown at the corner of a tower. The deposited energy is redistributed between this and other three adjacent towers. Except the small cracks between tiles, a region of low efficiency along the edge of a scintillator tile was also introduced. The widths of this region was taken to be 0.7 cm, and the drop of efficiency is 25%. Fig.9 shows the summed energy deposited in the four towers, as the function of the distance from the "corner" of a tower. A dramatic drop in the value of the deposited energy is observed at the distances smaller than 1.5 cm.

These distributions allow one to estimate the total surface of the region where the EEMC characteristics are disturbed by the "edge" effects.

* Total surface of EEMC $\simeq$ 13.2 m^2.

Surface of one 30^o–module = 1.1 m^2 = 11000 cm^2.

* Areas with 2 cm width near the radial wall, at both sides of the module, surface = $560cm^2$.

Areas 1.5 cm width, at both sides of the 6^o tile (if they are along the radius of the module), surface = 1.5cm * 140 cm * 2 * 4 = 1680 cm^2.

* (560 + 1680) / 11000 = 0.20

This means, that about 20% of all EEMC showers need corrections in the sense that though information is not completely lost here, the simple relation between the energy of the incident particle (γ or electron), and the tower response, is not valid. These distortions are, probably, correctable with the help of additional information about the position of a shower relatively to inefficient regions. The Shower Max data could be used to provide this position information.

5 EEMC : problem of the TPC Wheel.

As compared to the Barrel EMC, the End–cap EMC has an extra-complication, that probably will make the EEMC data processing more complex. Just in front of the EEMC, the TPC End-cap and TPC support structures are located. Made of aluminium, the TPC wheel has a rather complicated structure. Obviously, the quantity of dead material (in some places up to 2 radiation lengths) in front of the calorimeter could distort the calorimeter response.

A special study was made to estimate the range of possible distortions. This was done in the aGSTAR framework, as the geometrical description of the TPC structures in the aGSTAR files is very detailed. This is shown in Figures 10 and 11.

To get the quantity of dead material in front of the EEMC, the TPC was traced with geantinos in the range $0 < \eta < 2$ and $0 < \phi < 2\pi$. The results are shown in Fig.12. The average thickness of the material in front of the EEMC turned out to be 0.72 rad.length (assuming the flat distribution of incoming particles over $1 < \eta < 2$). This is a relatively large number, especially comparing with the the flat distribution of the material in front of BEMC : 0.19 rad.length. The peak of 2.25 rad.length around η=1 is troubling; though it is exactly the region of the gap between the BEMC and the EEMC where the particles are not detected; or produced showers are distorted.

To study the influence of the TPC Wheel on the characteristics of the detected particles, the EEMC response was simulated for 2000 photons with 10 GeV energy, with a uniform distribution over the EEMC acceptance. The simulations were performed twice : in a geometrical configuration with both the TPC and the EEMC , and in a configuration with the EEMC only.

With extra-material in front of the EEMC, some γ's convert before they reach the EEMC. On Figs.13a,b the distributions of the number of hits in the *first* sensitive layer of the EEMC are shown. The high multiplicity tail of the distribution obtained with the TPC is the result of these "early" showers.

In the configuration TPC+EEMC, all the events were divided into two classes :

– the cases when the number of hits in the first layer was $n_{hit_1} \leq 2$, and

– the cases when $n_{hit_1} > 2$.

The cases with a small number of hits in the first layer were assumed to belong to photons passing the TPC Wheel without initiating a shower. This assumption appears reasonable, as the average characteristics of the EEMC showers produced by these particles are quite similar to those obtained from the data set without the TPC.

The second class consists of those cases when the shower starts before the EEMC.

The difference between these two classes is caused by the presense of the TPC Wheel. The distributions of deposited energy in active EEMC layers are shown in Figs.13 c,d. The mean value of the deposited energy is shifted down for events with "early" showers, the relative shift in the deposited energy is **3%**.

The energy resolutions for these two cases are also different. For the particles with "early" showers, the resolution turned out to be $0.21/\sqrt{E}$, whereas for "normal" particles it is $0.18/\sqrt{E}$, i.e. the *relative* change is about **15%**. We studied the 10 GeV γ's more thoroughly, as this energy is of order of magnitude of the energy of γ's from the reaction $\gamma^* + jet$.

The γ's from ordinary *pp*–interaction have much lower energies, and the changes in energy resolution are more dramatic. For 1 GeV γ's, the relative shift of deposited energy is **11%**, and the energy resolution changed from $0.18/\sqrt{E}$ to $0.26/\sqrt{E}$, i.e. relative change in the resolution is about **40%**.

Another important question is how the presense of the TPC Wheel influences the shower profiles in the EEMC ShowerMax Detector (SMD). Whereas the average number of hits in the SMD remains almost the same in both cases (Fig.14), the width of the SMD profiles increases for the "TPC showers". The dispersion of each individual shower profile (along the y-axis) was calculated, and the resulting distributions of shower dispersions are shown on Fig.15. For particles with showers that start in the TPC Wheel, the average SMD profile dispersion turns out to be 0.4 cm larger, i.e. the average increase in the full width of the shower profile in the SMD (x- or y- axis projection) is around 1 cm. The dispersion of the SMD profiles is close to the Moliere radius R_m for lead (even taking into account the longitudinal segmentation of EEMC and presense of light scintillator). The widening of the SMD profiles decreases the probability to resolve the two–photon events using the SMD.

The obtained data shows that the presense of the TPC Wheel in front of the EEMC influences the EEMC response, energy resolution and the shape of the SMD profiles [9].

The following design solutions could be proposed to avoid the bigger future troubles.

First, the 30^o EEMC modules should be aligned with the TPC Wheel. It means that the "first" EEMC module should cover the angle from -15^o to $+15^o$. Then the spokes of the TPC Wheel will coincide with the walls between the EEMC modules. The EEMC inefficient regions will become even more inefficient (see Fig.12, right plot) but the rest of the EEMC will stay more or less undisturbed.

Second, the information from the first sensitive layer of the EEMC would be very desirable. A separate read-out of this layer will raise the cost of the project, and probably could not be implemented in the very beginning of the experiment. But the possibility to do this in the future should be incorporated in the EEMC design : extra–fibers and extra–space for PMT and electronics should be provided.

6 Small comment : γ's and jets.

The proposal to install the EEMC is motivated by the need of extending the STAR effective acceptance for jets and photons. Until now, the efficiency of the jet–finding algorithm was studied for jets with $0.3 < \eta < 0.3$, when most of the jet particles are inside the BEMC acceptance [7].

[9] The relative number of γ's that start a shower inthe TPC Wheel is $\sim$25% of all passing γ's. This number is lower than expected from quantity of extra material in front of the EEMC, because the average conversion length for γ's requires about 0.7 radiation length. But for electrons, more than half of them will start showers in the TPC Wheel.

Based on these studies, Tom LeCompte estimated [10] the energy resolution for reconstructed jets is $\sim 30\%$. For the jets with higher average η, i.e. smaller θ, the situation seems to be more complicated.

Some of the jet particles will be "invisible" in the detector due to the gap between the BEMC and the EEMC in the region around $\eta = 1$, more will disapper in a region $\eta > 2$.

Also, the EMC jet–finding algorithm uses data from the STAR tracking system, i.e. charged track parameters from the TPC. Charged tracks at large η are crossing a smaller number of TPC pads, and their curvature is also smaller,
as compared with tracks at $\eta \sim 0$.

For these reasons the energy resolution for jets with $\eta > 1$ will require special study.

7 Summary and Conclusion.

At the level of GEANT simulations, the EEMC detector shows no peculiar behavior, and its characteristics are close to those expected from similar lead-scintillator calorimeters. Nevertheless, some regions of the EEMC are distorted in the sense that the characteristics of the EEMC in these regions can deviate from the expected. Probably, the information from the Shower Max detector should be used at an early stage of EEMC data processing to correct for these deviations.

At the design level, the additional preparations for possible read-out of the first EEMC sensitive layer should be done. Also, the proper aligning of the EEMC modules with the TPC Wheel should be done as well.

We would like to suggest to discuss in the Collaboration the idea of building and testing the small prototype of EEMC, with all realistic features, including walls, cracks and the dead material in front of it. This would allow one to make the simulations more sophisticated and more representative of the real situation. Also, this would allow one to simulate not only the physical processes in the calorimeter itself, but extend the simulation through the analysis chain.

* * *

[10] See Chapter "EMC and Spin Frequently Asked Questions" at
http://sgi12.hep.anl.gov/~lecompte/Public/star/emcsim.html

In conclusion, we would like to thank Pavel Nevski for his explanations and assistance he gave us during the study of the new version of aGSTAR.

One of the authors (K.M.) is highly appreciative of the interest of Tim Hallman about the subject of this study, and his help and hospitality during the author's visit to Brookhaven National Laboratory. Also, his special thanks go to Valery Shvetsov (JINR,Dubna), for the pertinent explanations about the details of EEMC design.

References

[1] B.Adeva et al., SMC Collaboration,
"Measurement of the spin–dependent structure function g1(x) of the proton",
Phys.Lett. B329 (1994) 399.

B.Adeva et al., SMC Collaboration,
"Combined analysis of world data on nucleon spin structure functions",
Phys.Lett. B320 (1994) 400.

[2] R.W.Robinett, "Prospects for spin physics at RHIC",
Preprint ANL–HEP–CP–95-28; PSU/TH/160, 1995.

[3] HMC Collaboration (Proposal of the experiment),
"Semi–inclusive muon scattering from a polarized target",
CERN/SPSLC 95–27, CERN, 1995.

[4] Private communication. The PSU proposal to build an End-cap calorimeter for STAR is available upon request from Steve Heppelmann.

[5] The drawings of the STAR Integration Group are available at :
http://me62.lbl.gov:8001/STAR/TEXT/star1.3.html
Please, pay special attention to drawings SIM140–A–1 and SIM160–A–1.

[6] P.Nevski, "Advanced geometry Interface for GSTAR", to be published.
Now available in ~nevski/public/star/doc/agstar.ps

[7] B.Christie, K.Shestermanov,
"Efficiency of modified UA1 jet reconstruction algorithm in pp, pA and AA collisions at STAR", STAR Note 196.

[8] R.K.Bock et al., "Data analysis techniques for high–energy physics experiments",
Ed. M.Regler, Cambridge University press, 1990.

[9] U.Amaldi, "Fluctuations in Calorimetry Measurements", Physica Scripta, 23 (1983) 409.

[10] D.J.Fisher, "Rules of Thumb for Physical Scientists",
Trans Tech Publications, Switzerland, 1988.

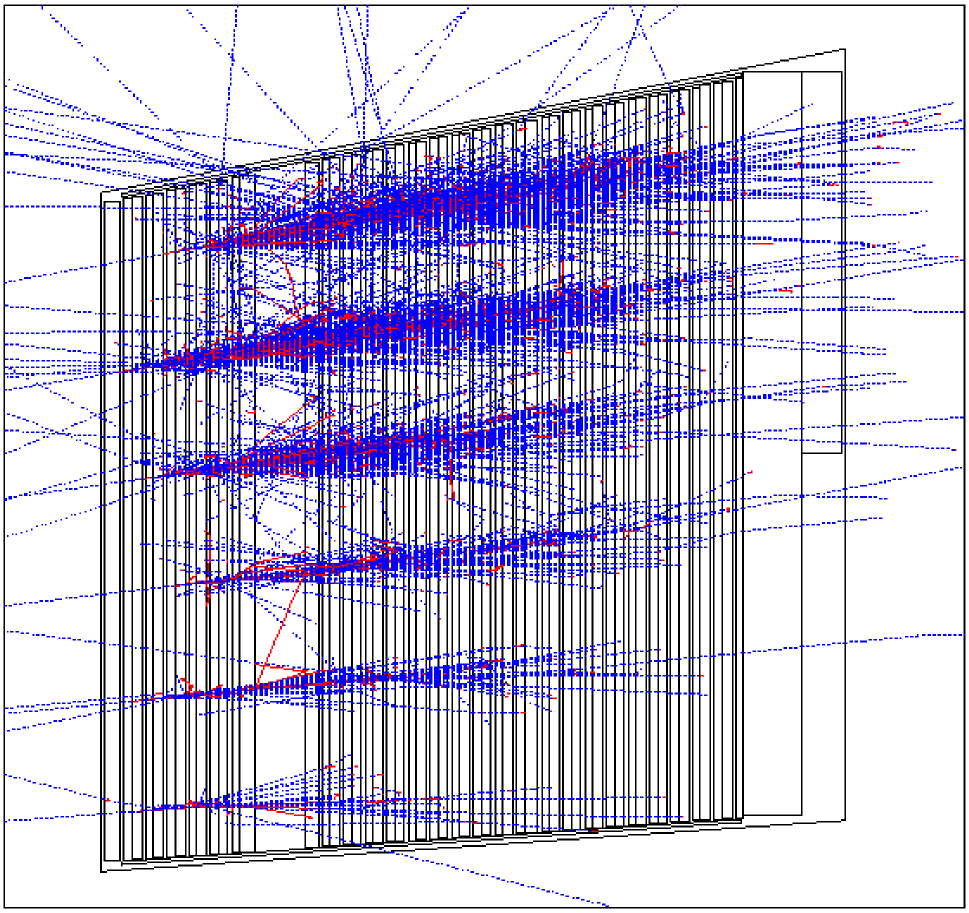

Figure 3. *Electromagnetic showers in EEMC, initiated by* γ*'s of various energies — as seen in Geant. Please, note – the relative vertical and horizontal scale of the picture are different from the proposed EEMC. This is done only for presentation purpose. The EEMC in GEANT had the correct dimensions.* γ's energies :

$\longrightarrow \diamond$ 15 GeV (top of the figure);

$\longrightarrow \diamond$ 10 GeV;

$\longrightarrow \diamond$ 5 GeV;

$\longrightarrow \diamond$ 2 GeV;

$\longrightarrow \diamond$ 1 GeV;

$\longrightarrow \diamond$ 0.5 GeV (bottom of the figure).

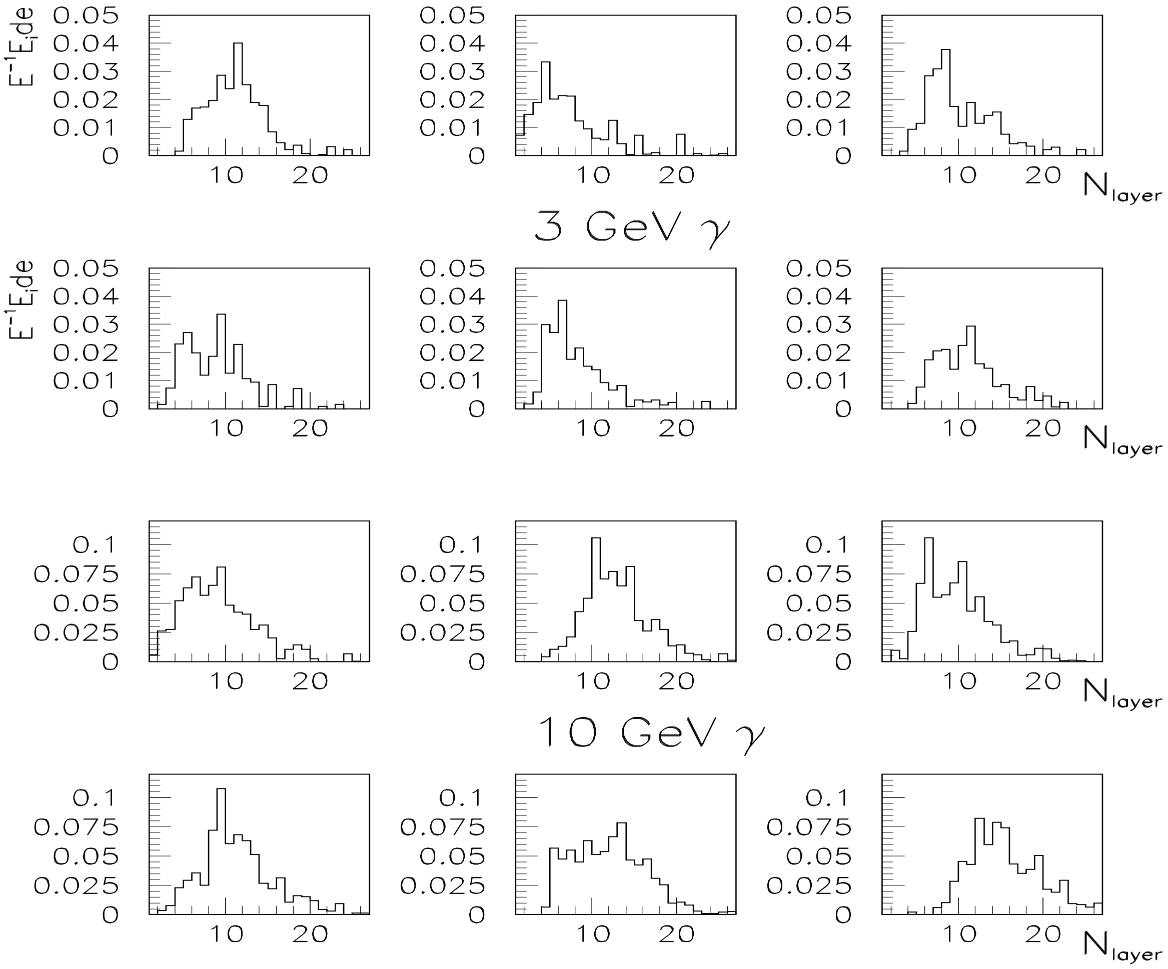

Figure 4. *Examples of the electromagnetic shower profiles in EEMC. Showers are shown for γ's energies 3 and 10 GeV.*

.

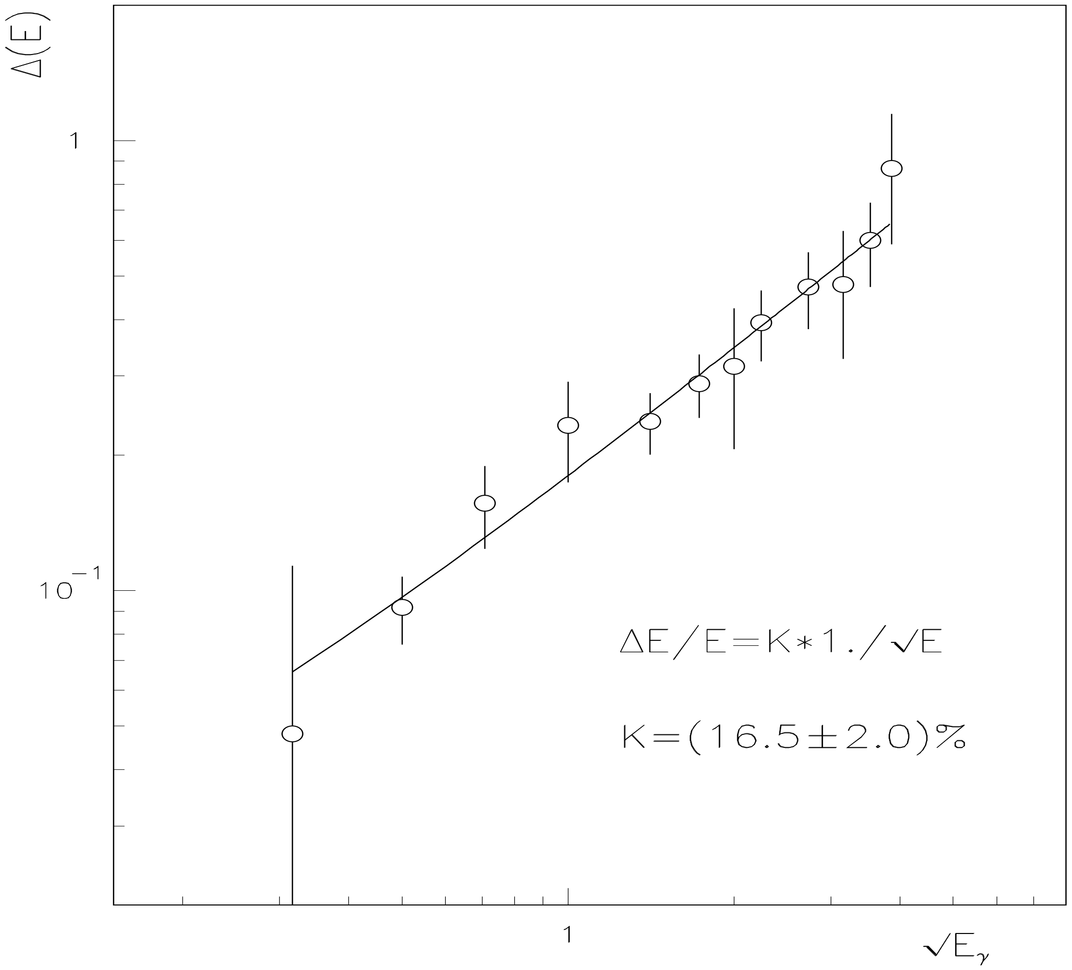

Figure 5. *Absolute dispersion* ΔE *(in GeV) of energy distribution in EEMC, is shown as the function of* $\sqrt{E_\gamma}$ *of incident* γ*'s. The fit gives the energy resolution of EEMC. Error bars show the rms in values of* ΔE *.*

.

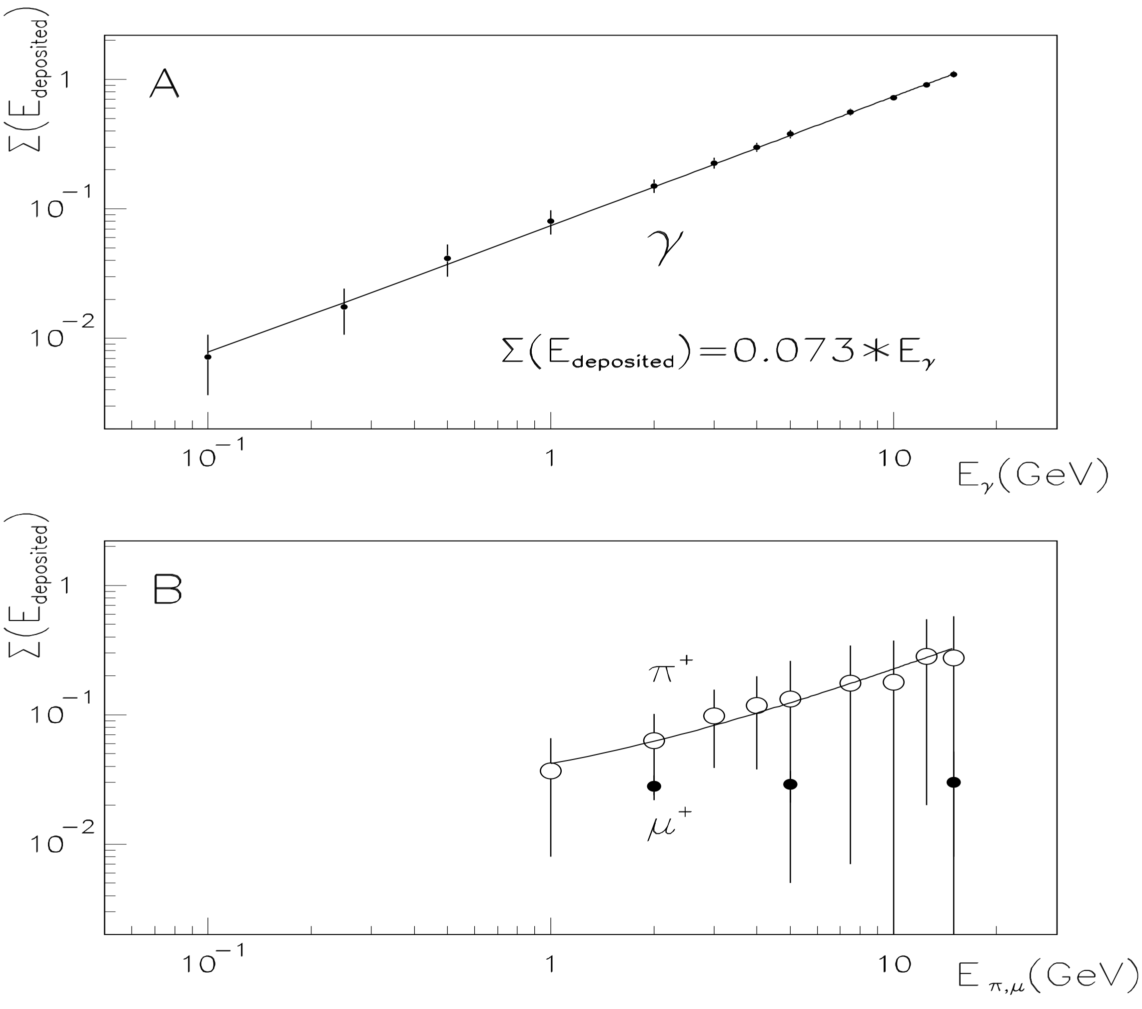

Figure 6.

Fig.6.a. – the dependence between deposited energy in EEMC and the energy of γ's.

Fig.6.b. – the dependence between deposited energy in EEMC and the energies of π^+ and μ^+. Error bars represent the energy fluctuations in EEMC for π–mesons.

.

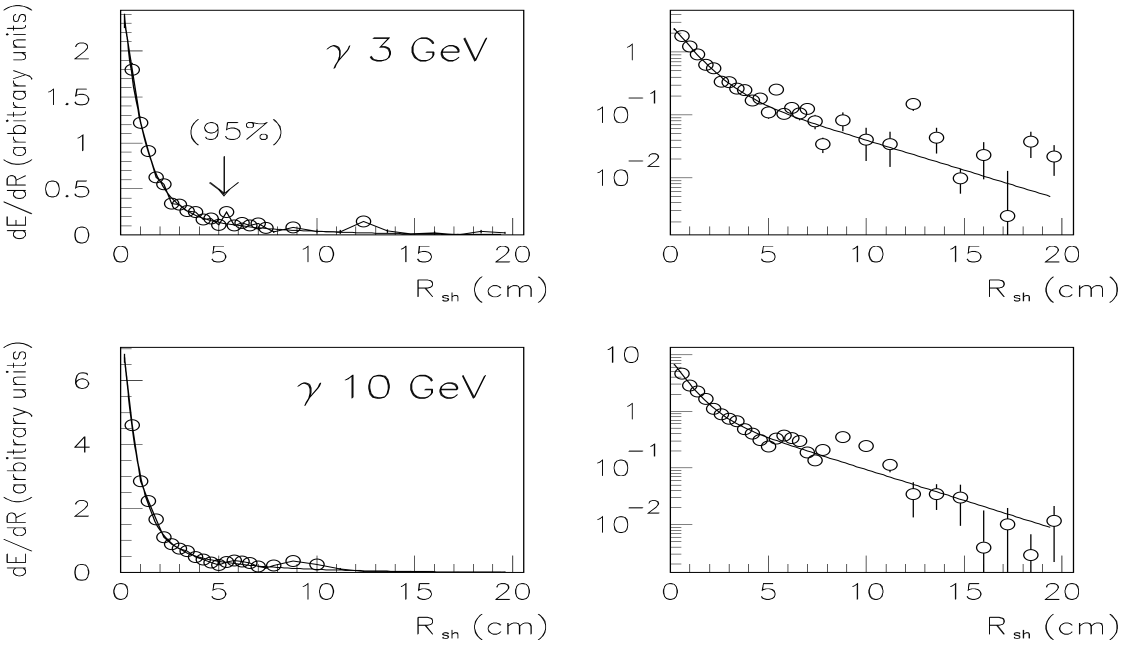

Figure 7.

The radial distribution of the electromagnetic shower energy. The distribution is integrated over all EEMC active layers. R_{sh} is the distance in cm between the position of a hit and the shower axis. The distributions are shown both in linear and logarithmic scales. This allows one to see the existence of the two slopes in the distributions.

The energy of the γ's are 3 and 10 GeV. An arrow indicate the radius of a cylinder, inside which 95% of all shower energy is concentrated.

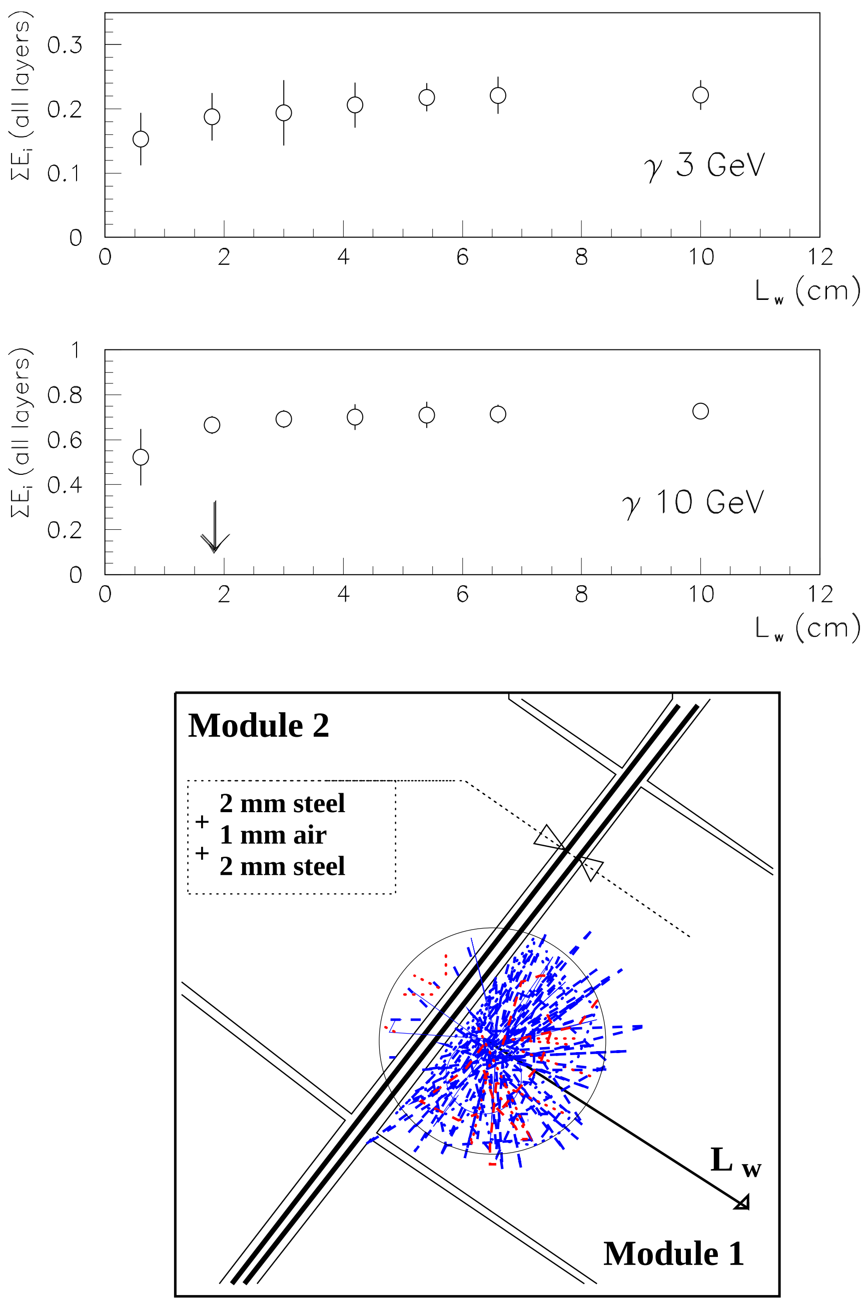

Figure 8. *Energy deposit (in GeV) in EEMC is shown as a function of the distance between the shower center and the support wall (steel wall between the EEMC modules).*

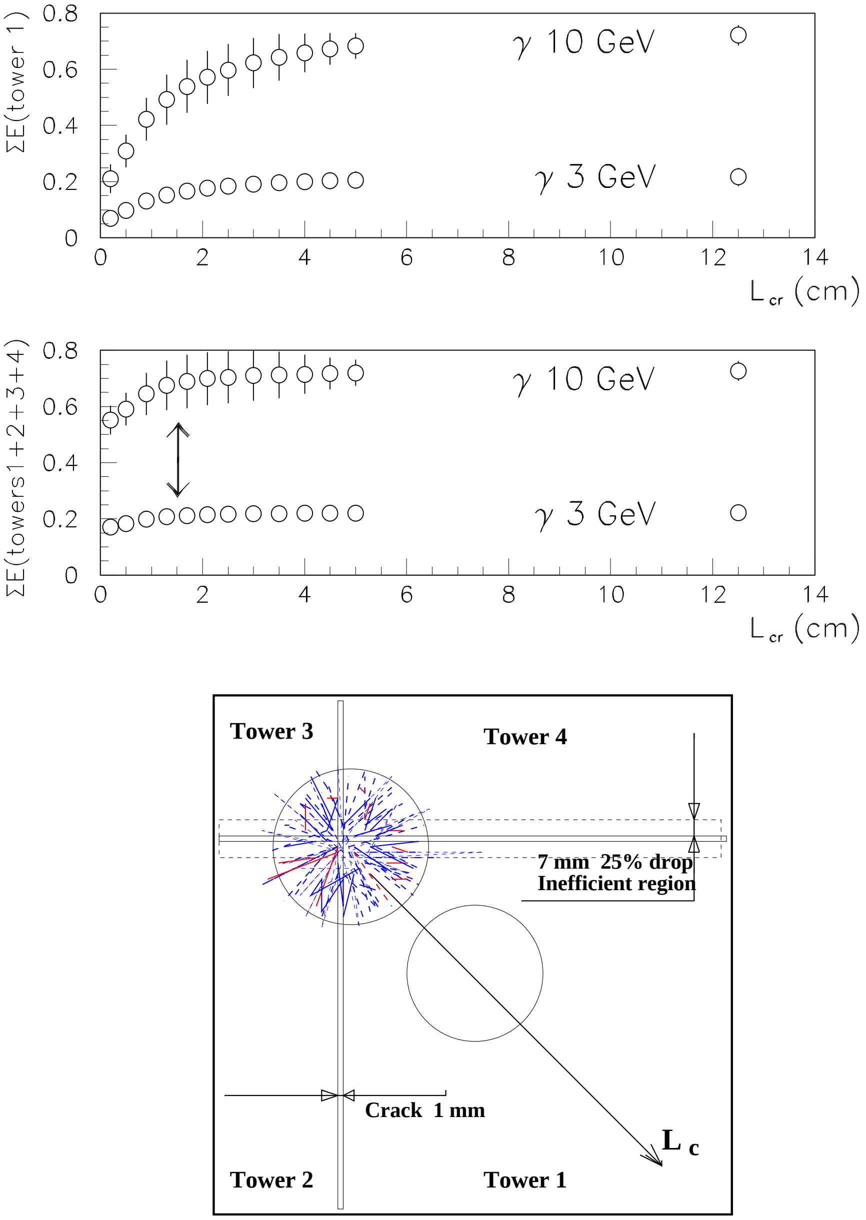

Figure 9. *Shower is shown close to the corner of Tower 1.*

Some shower energy is seen in other 3 adjacent towers. Energy deposit (in GeV) is presented as a function of the distance between the shower center and the corner of a tile.

Upper picture : deposited energy in Tower 1.

Lower picture : sum of deposited energies in all 4 towers.

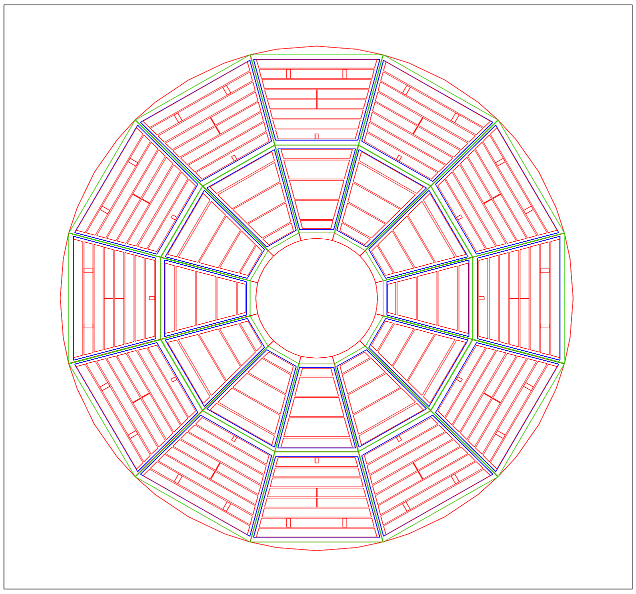

Figure 10. *Aluminium sector structures of TPC Endcap.*

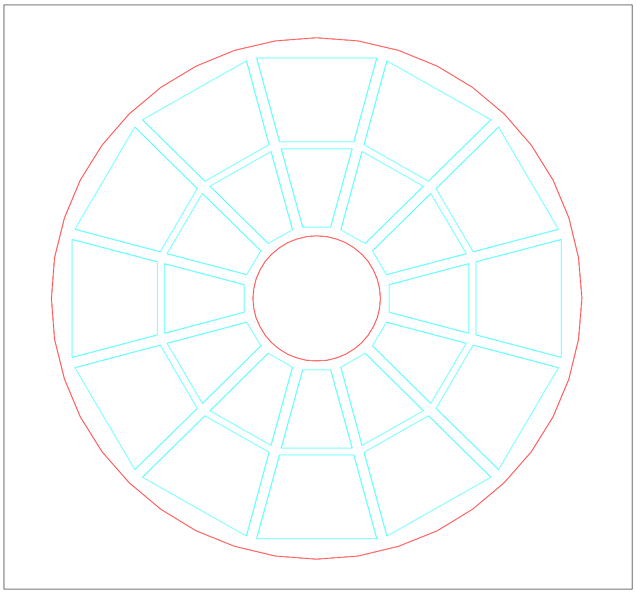

Figure 11. *Aluminium support wheel of TPC Endcap.*

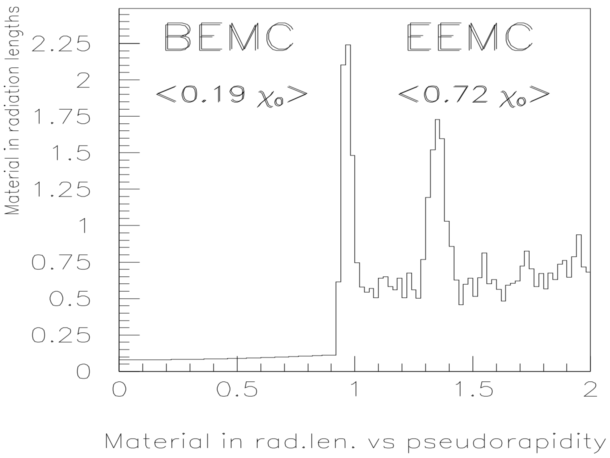

Figure 12. *Distributions of extra material (in units of radiation length) in front of BEMC and EEMC, as functions of* η *and* ϕ.

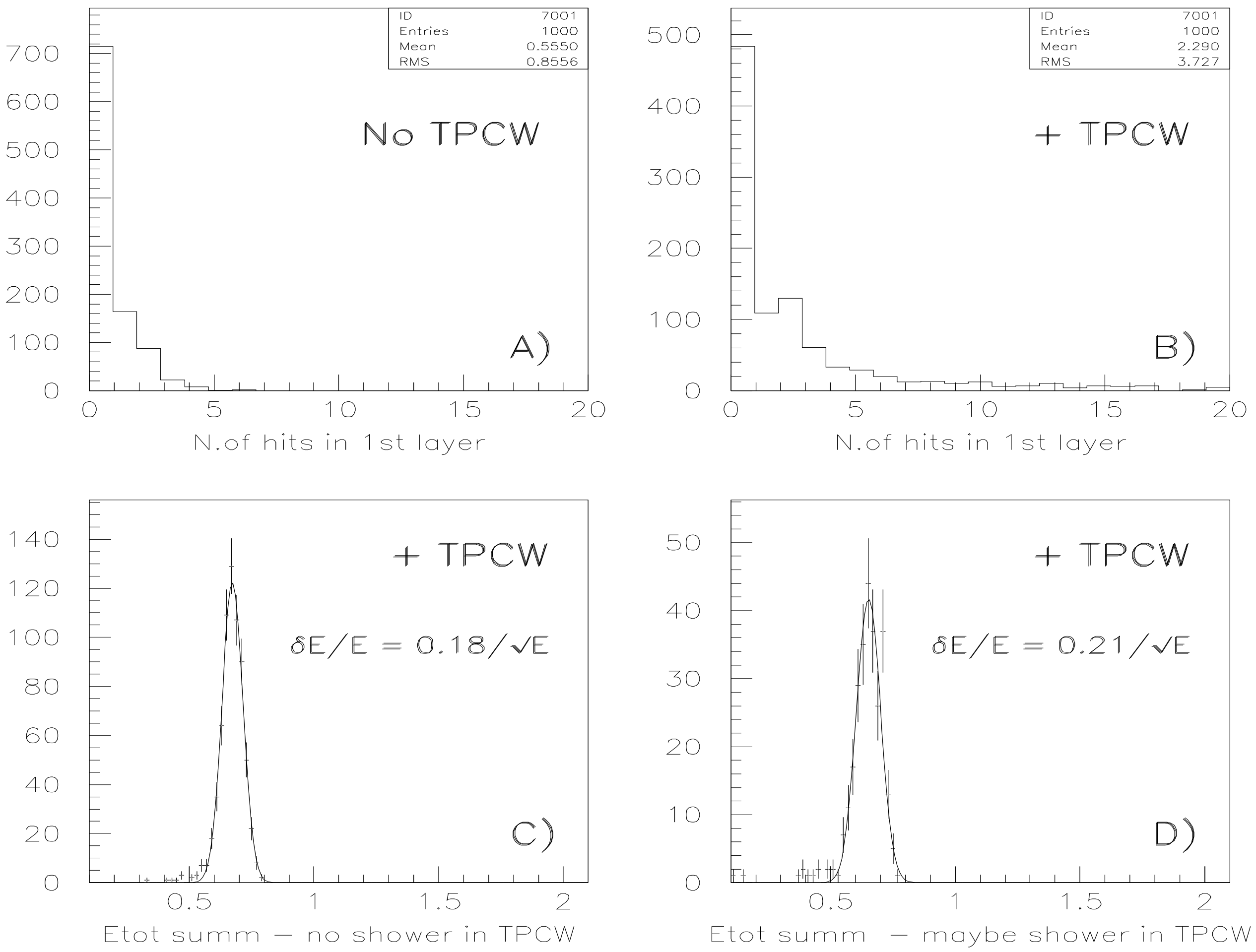

Figure 13. *Results for 10 GeV γ–showers in EEMC :*

A) Distribution of number of hits in the first active EEMC layer. No TPCWheel.

B) Distribution of number of hits in the first active layer of EEMC.

TPCWheel is in front of EEMC.

C) EEMC energy resolution, assuming no showers in TPCWheel.

D) EEMC energy resolution, assuming an interaction in TPCWheel.

.

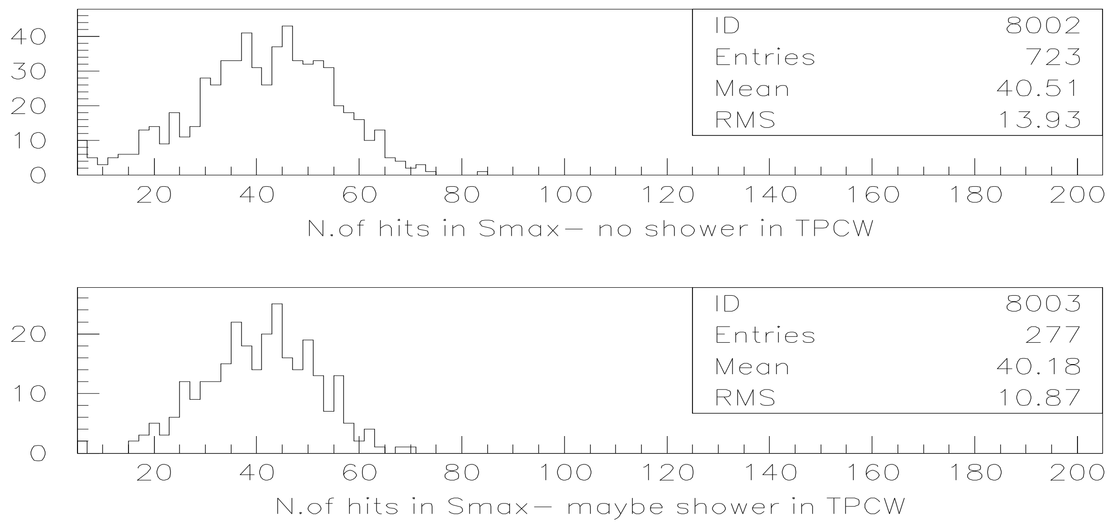

Figure 14.*Distributions of number of hits in EEMC ShowerMax Detector. Upper picture is for showers with vertex in EEMC. Lower picture is for showers with vertex in TPCWheel.*

.

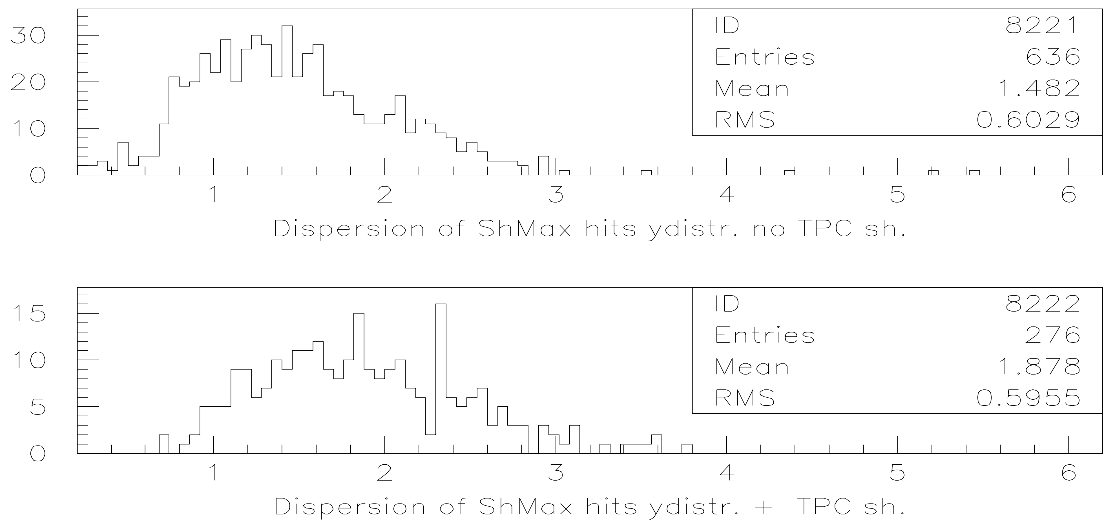

Figure 15.*Distributions of dispersions of ShowerMax profiles (along y–axis). Upper picture is for showers with vertex in EEMC. Lower picture is for showers with vertex in TPCWheel.*